nature nanotechnology
LETTERS

Single-nanocrystal sensitivity achieved by enhanced upconversion luminescence

Jiangbo Zhao[1], Dayong Jin[1]*, Erik P. Schartner[2], Yiqing Lu[1], Yujia Liu[1,3], Andrei V. Zvyagin[1], Lixin Zhang[1], Judith M. Dawes[1], Peng Xi[3,4], James A. Piper[1], Ewa M. Goldys[1] and Tanya M. Monro[2]

Upconversion nanocrystals convert infrared radiation to visible luminescence, and are promising for applications in biodetection[1–3], bioimaging[4–7], solar cells[8–10] and three-dimensional display technologies[8,9,11]. Although the design of suitable nanocrystals has improved the performance of upconversion nanocrystals[10,12–14], their emission brightness is limited by the low doping concentration of activator ions needed to avoid the luminescence quenching that occurs at high concentrations[15,16]. Here, we demonstrate that high excitation irradiance can alleviate concentration quenching in upconversion luminescence when combined with higher activator concentration, which can be increased from 0.5 mol% to 8 mol% Tm^{3+} in $NaYF_4$. This leads to significantly enhanced luminescence signals, by up to a factor of 70. By using such bright nanocrystals, we demonstrate remote tracking of a single nanocrystal with a microstructured optical-fibre dip sensor. This represents a sensitivity improvement of three orders of magnitude over benchmark nanocrystals such as quantum dots[17].

Lanthanide-doped upconversion nanocrystals[8,9] are typically doped with ytterbium (Yb^{3+}) sensitizer ions, which absorb infrared radiation and non-radiatively transfer their excitation to activator ions such as erbium (Er^{3+}), thulium (Tm^{3+}) or holmium (Ho^{3+}). Although recent advances in synthesis have led to accurate control of upconversion nanocrystal morphology, crystal phase and emission colours[7,11,15,16,18–21], it has been difficult to achieve strong upconversion luminescence. Attempts to overcome this problem include coating nanocrystals with an inert/active shell to minimize surface quenching[12,14,22,23], or using noble metal nanostructures to enhance the energy transfer rate by surface plasmons[24,25]. However, these approaches do not address the intrinsic limitation of concentration quenching[15,16,18], where brightness decreases with increasing dopant density beyond the optimal concentration threshold. The optimal Tm^{3+} concentration in $NaYF_4$ host lattices is low, in the range of ~0.2–0.5 mol% at excitation irradiance below 100 W cm^{-2} (with ~20–40 mol% Yb^{3+})[16,26–29]. Such nanocrystals have small numbers of activators and therefore produce weak upconversion emission.

Here we present evidence that upconversion luminescence can be significantly enhanced by using much higher activator concentrations under relatively high-irradiance excitation. We have found that this previously unexplored regime achieves a new balance between the sensitizers, activators and excitation irradiance, and can overcome the widely reported concentration quenching in upconversion[15,16,18,26–29]. As a result, it has been possible to realize high bright upconversion luminescence in 8 mol% Tm^{3+}-doped $NaYF_4$ nanocrystals co-doped with 20 mol% Yb^{3+}. Their high brightness originates from a combination of high excitation intensity, increased activator concentration, and accelerated sensitizer–activator energy transfer rate arising from the decreased average minimum distance between adjacent Ln^{3+} ions. This significantly enhanced upconversion has enabled the remote detection of a single nanocrystal using a fibre dip sensor.

Hexagonal-phase $NaYF_4$ nanocrystals were synthesized with Tm^{3+} concentrations in the range ~0.2–8 mol% co-doped with 20 mol% Yb^{3+} (Supplementary Section S1 and Fig. S1). A single-mode continuous-wave 980 nm diode laser beam launched into a suspended-core microstructured optical fibre (Fig. 1) produced excitation irradiance values of up to 2.5×10^6 W cm^{-2}. The uniform ~40 nm nanocrystals dispersed in cyclohexane (39 pM) were drawn into the holes in the fibre for upconversion luminescence measurements (Supplementary Section S2). This brings the nanocrystals into the vicinity of sufficiently high intensity guided light, and also provides a platform suitable for efficiently collecting their emission. At 2.5×10^6 W cm^{-2} irradiance, we observed that the 8 mol% Tm^{3+} nanocrystals generate a previously unreported bright upconversion emission that is much stronger than in 0.5 mol% Tm^{3+} nanocrystals (the 802 nm emission is increased by a factor of 70, Fig. 1c). In contrast, at a low excitation of 10 W cm^{-2}, our results (Supplementary Fig. S2) show that the upconversion intensity as a function of Tm^{3+} concentration first increases and then decreases above 0.5 mol% Tm^{3+}, consistent with previous reports[16,26–29]. This observation indicates that efficient upconversion emission can be realized at a high activator doping, but only when sufficient irradiance is provided (~1×10^6 W cm^{-2}, achieved in laser scanning microscopy). Sufficient excitation irradiance can unlock otherwise dark activators, thereby enhancing the upconversion brightness (Supplementary Fig S3). This effect is independent of nanocrystal size (from tens to several hundreds of nanometres), surface conditions and synthesis conditions (Supplementary Sections S3, S4, Figs S3–S7).

To understand the relationship between the upconversion signal, activator concentration and excitation irradiance, we collected a matrix of power-dependent (1.6×10^4 W cm^{-2} to 2.5×10^6 W cm^{-2}) luminescence spectra for same sized ~40 nm upconversion nanocrystals at varying Tm^{3+} concentrations. The spectra, which are similar to those in Fig. 2b were decomposed into individual Gaussian peaks (Fig. 2c). These were divided into three groups according to the initial Tm^{3+} levels: the $^3H_4$ group, comprising a single peak at 802 nm, the $^1G_4$ group, with 650 nm and 480 nm peaks, and the $^1D_2$ group, with peaks at 455 nm, 514 nm, 744 nm and 782 nm (see Fig. 2a for a simplified diagram of transitions in the Yb^{3+}–Tm^{3+} system). The integrated intensity ratios of the $^1D_2$

---

[1]Advanced Cytometry Laboratories, MQ Photonics Research Centre and MQ BioFocus Research Centre, Macquarie University, Sydney, New South Wales 2109, Australia, [2]Institute of Photonics and Advanced Sensing and School of Chemistry and Physics, University of Adelaide, Adelaide, South Australia 5005, Australia, [3]School of Biomedical Engineering, Shanghai Jiao Tong University, Shanghai, China, [4]Department of Biomedical Engineering, College of Engineering, Peking University, Beijing 100871, China. *e-mail: dayong.jin@mq.edu.au

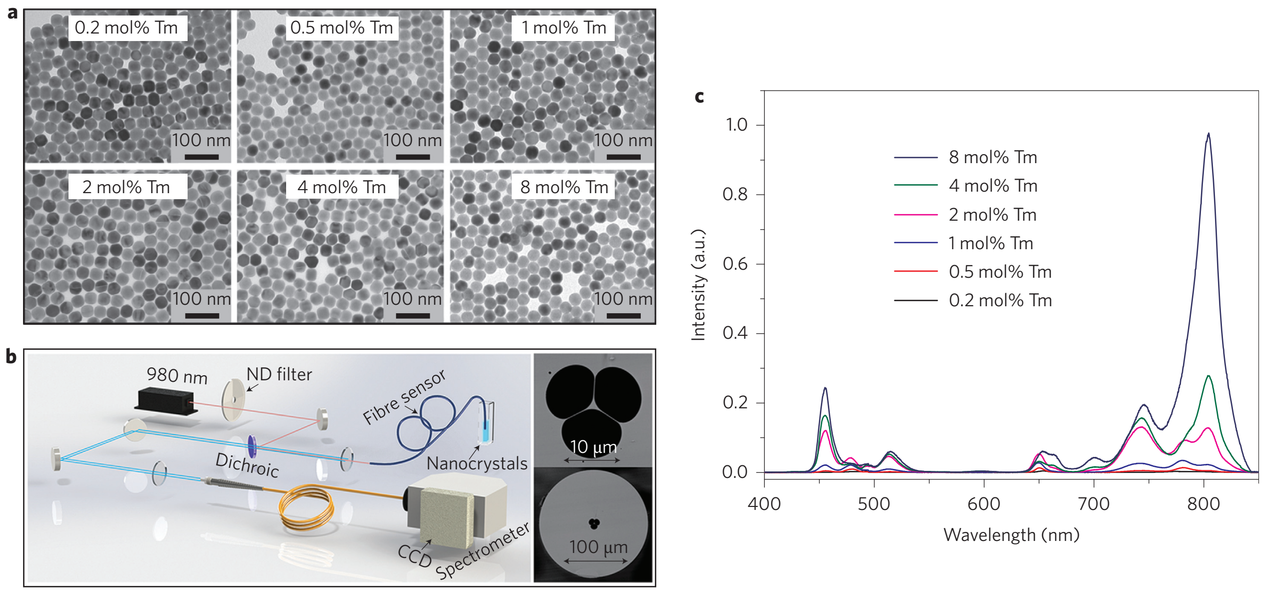

Figure 1 | Highly Tm^{3+}-doped $NaYF_4$ nanocrystals exhibit enhanced upconversion in a suspended-core fibre. a, Transmission electron microscopy images of monodispersed $NaYF_4$:Yb/Tm nanocrystals at different doping levels. All nanoparticles have a similar average size with a narrow size distribution. **b**, Schematic of the experimental configuration for capturing upconversion luminescence of $NaYF_4$:Yb/Tm nanocrystals using a suspended-core microstructured optical-fibre dip sensor. The continuous-wave 980-nm diode laser is targeted at the suspended core. Light propagates along the length of the fibre and interacts with the upconversion nanocrystals located within the surrounding holes. The excited upconversion luminescence is coupled into the fibre core and the backward-propagating light is captured by a spectrometer. Inset: scanning electron microscope images showing a cross-section of the F2 suspended-core microstructured optical fibre at different magnifications. The fibre outer diameter is 160 μm with a 17 μm hole and 1.43 μm core. **c**, Upconversion spectra of a series of $NaYF_4$:Yb/Tm nanocrystals with varied Tm^{3+} concentrations under an excitation irradiance of 2.5×10^6 W cm^{-2}, showing a steady increase in upconversion luminescence with increasing Tm^{3+} content from 0.2 mol% to 8 mol%.

to $^3H_4$ and $^1G_4$ to $^3H_4$ groups (Fig. 2d) show a decreasing contribution of emissions from the $^1G_4$ and $^1D_2$ groups with increasing Tm^{3+} content compared to $^3H_4$ emission. This suggests that the respective population ratios of $^1D_2$ and $^1G_4$ levels to $^3H_4$ decrease in these conditions, to a point where the 8 mol% Tm^{3+} nanocrystals mainly produce the $^3H_4$ (802 nm) emission within our excitation range. We also note that the emission ratios of $^1G_4$:$^3H_4$ and $^1D_2$:$^3H_4$ increase with excitation irradiance in all samples. This suggests that, with increasing excitation irradiance, the population of $^1D_2$ and $^1G_4$ levels increases faster than the population of $^3H_4$. These trends also suggest that a low activator concentration causes an energy transfer bottleneck: at increasing excitation powers the $^3H_4$ level eventually reaches its full capacity to release the 802 nm emission energy (Fig. 2e), and, in order to release any additional energy transferred from Yb^{3+}, the higher energy level emissions in Tm^{3+} ($^1G_4$ and $^1D_2$) become progressively activated. At higher Tm^{3+} concentrations the decay rate of the $^3H_4$ population increases, and this shifts the bottleneck to proportionately higher excitation energies.

Moreover, we have confirmed that the absolute conversion efficiency strongly increases with increasing irradiance, which is attributed to increased excited-state populations of sensitizer and activator ions. The absolute conversion efficiency is defined as the ratio of the emitted to absorbed power (Supplementary Section S5 and Fig. S8)[14]. The absolute conversion efficiency in the low concentration (0.5 mol%) sample reaches a plateau at 3×10^2 W cm^{-2}, whereas in the high concentration (4 mol%) sample it continues to increase within this range. We also measured the power-dependent relative upconversion efficiency for the different nanocrystal samples (Fig. 3a). Increasing the excitation irradiance from 1.6×10^4 W cm^{-2} to 2.5×10^6 W cm^{-2} enhances the overall upconversion luminescence intensity by factors of 5.6, 71 and 1,105 for 0.5 mol%, 4 mol% and 8 mol% Tm^{3+}, respectively. Additionally, this figure indicates that the partitioning of excitation energy flux between the 'effective' 980 nm quanta actually producing upconversion and those 980 nm quanta that are lost on other processes (such as various non-radiative recombination and unobserved emissions) changes dramatically with excitation irradiance and concentration of Tm^{3+} ions. Importantly, at high excitation and high Tm^{3+} doping level, the fraction of excitation energy producing upconversion emission is increased. This shows that upconversion is more efficient at high excitation and for high Tm^{3+} doping. The effect is observed to be especially strong for the 8 mol% Tm^{3+} samples, as is evident from the extremely steep slope above 2×10^6 W cm^{-2} excitation irradiance. Figure 3b shows the same integrated upconversion intensity per Tm^{3+} ion for different Tm^{3+} doping levels. Although the observation of significant enhancement in upconversion intensity from 0.2 mol% to 1 mol% may be due to the fact that upconversion from five photon excitations, previously reported in 0.2 mol% Tm^{3+} (refs 30–32), was not collected in this work, the increase from 1 mol% to 2 mol% clearly shows that the energy transfer efficiency from Yb^{3+} sensitizers to Tm^{3+} activators has been significantly enhanced. This work has therefore shown that the decreased excited sensitizer-to-excited activator distance has indeed increased the energy transfer efficiency, which makes a significant contribution to enhancing the overall conversion efficiency.

To verify that increasing the excitation irradiance enhances the upconversion luminescence and changes the optimal activator/sensitizer concentration ratio, we formulated the rate equations in a generalized upconverting Yb^{3+}–Ln^{3+} system (Supplementary Section S6 and Fig. S9a). In our model the lanthanide ion (activator) is represented by three states—Ln_0, Ln_1 and Ln_2—with equal energy spacing $E_2 - E_1 = E_1 - E_0$, and the upconversion emission takes place from the excited Ln_2 state to the ground Ln_0 state. The lanthanide ions are excited by energy transfer from the excited states of Yb^{3+} (Yb_1) populated by transitions from the ground-state Yb_0, which have the same energy spacing of $E_1 - E_0$. Using our rate equations,

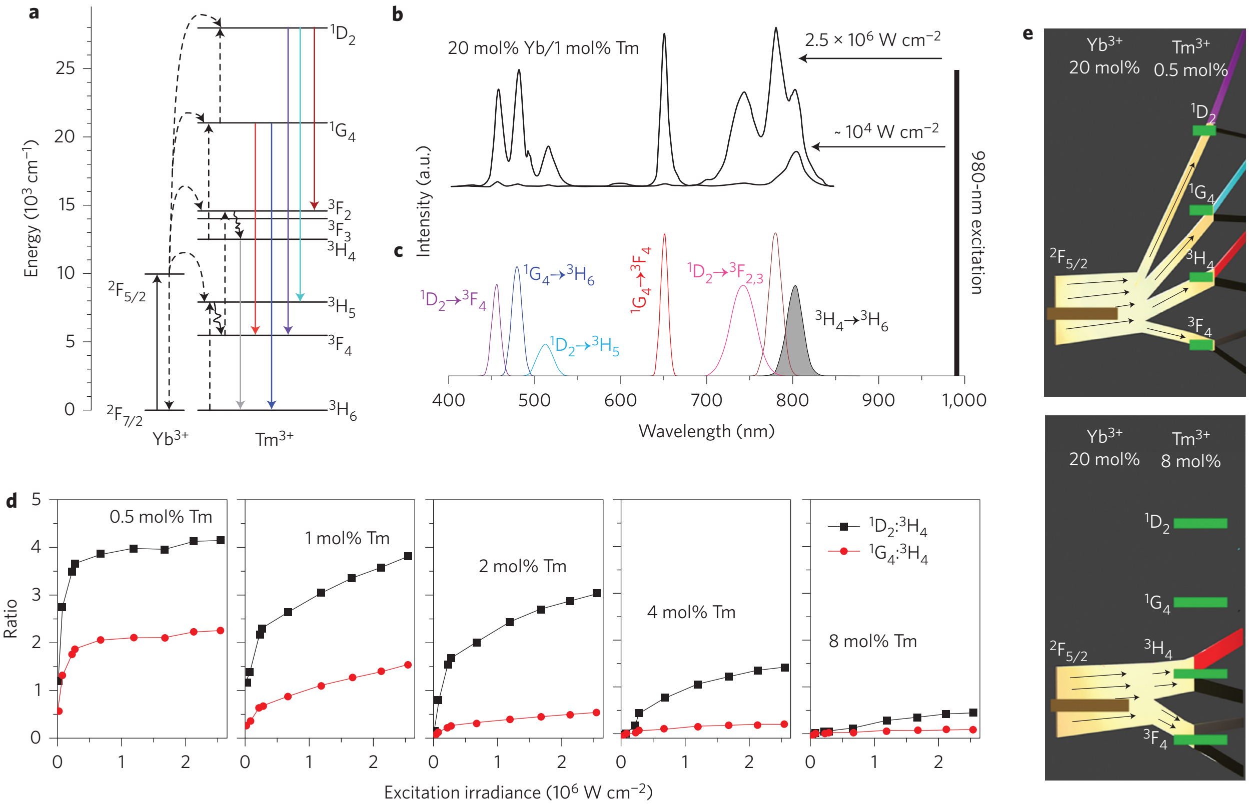

Figure 2 | Analysis of power-dependent multiphoton upconversion. a, Simplified energy-level scheme of NaYF$_4$:Yb/Tm nanocrystals indicating major upconversion processes. Dashed lines indicate non-radiative energy transfer, and curved arrows indicate multiphonon relaxation. **b**, Typical evolution of spectra for 1 mol% Tm^{3+} as a function of excitation, showing substantial growth of emissions from the $^1G_4$ and $^1D_2$ levels with increasing excitation from 1×10^4 W cm^{-2} to 2.5×10^6 W cm^{-2}. **c**, Decomposition of the spectra into individual Gaussian peaks. Integrated intensities are given by I_λ where λ is the peak wavelength. Different transitions are indicated by the colours shown in the energy-level scheme in **a**. For example, the shaded area represents the $^3H_4 \rightarrow {}^3H_6$ transitions. **d**, Intensity ratios of the $^1D_2$ to $^3H_4$ classes $(I_{455} + I_{514} + I_{744} + I_{782})/I_{802}$ and $^1G_4$ to $^3H_4$ classes $(I_{480} + I_{660})/I_{802}$ as a function of excitation irradiance. **e**, Diagram illustrating energy transfer between the ensemble of Yb^{3+} and Tm^{3+} ions and subsequent radiative and non-radiative pathways. Top (bottom) panels: low (high) Tm^{3+}/Yb^{3+} ratio. In the case of a low Tm^{3+}/Yb^{3+} ratio, the limited number of Tm^{3+} ions creates an energy transfer bottleneck, due to the limited capacity of Tm^{3+} to release energy from the $^3F_4$ and $^3H_4$ states. Thus, at increasing excitation, alternative energy loss channels (radiative and non-radiative) involving higher states $^1G_4$ and $^1D_2$ progressively switch on. Brown, excitation light; green, simplified energy levels; red, blue and purple, radiative energy flux; grey, radiative flux not observed in this work; black, non-radiative energy loss.

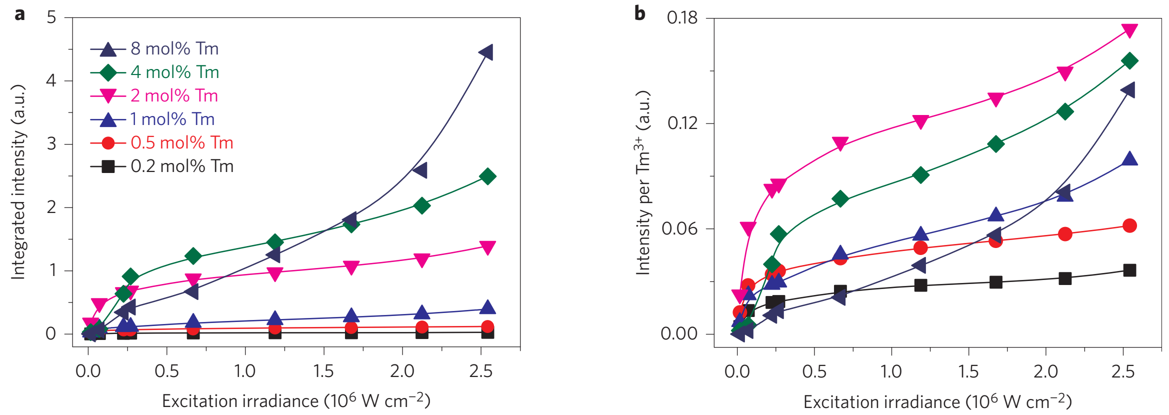

Figure 3 | Analysis of power-dependent upconversion efficiency. a, Integrated upconversion luminescence intensity (~400–850 nm) as a function of excitation irradiance for a series of Tm^{3+}-doped nanocrystals. All samples have the same volume and number of nanocrystals. **b**, As in **a**, but divided by the concentration of Tm^{3+} ions. Under an excitation irradiance of 2.5×10^6 W cm^{-2}, 2 mol% Tm^{3+} has the highest relative upconversion efficiency, whereas the strongest upconversion signal is observed in 8 mol% Tm^{3+} due to the larger number of activators available with sufficient excitation.

the population in the Ln$_2$ state is expressed in terms of the density of lanthanide ions in the ground state, the excited Yb^{3+} population, excitation irradiance and various intrinsic macroscopic rate constants, such as the energy transfer and upconversion rates. The experimental and simulated upconversion luminescence intensities show concentration quenching at low irradiance, but increase at

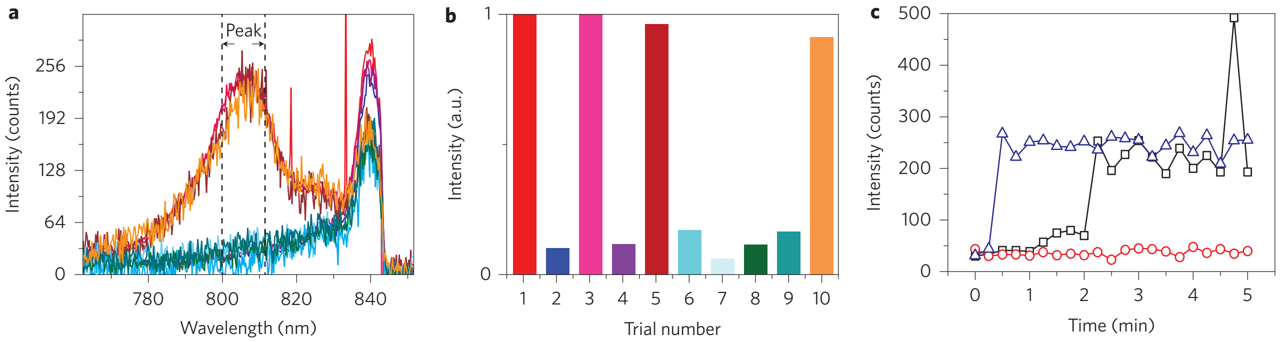

Figure 4 | Detecting a single nanocrystal in a suspended-core microstructured fibre dip sensor. a, Results of 10 trials of loading 3.9 fM nanocrystal solution into the fibre dip sensor. Four positive trials, shown in red, magenta, dark red and orange, show comparable ~800–810 nm emission peaks, and six trials result in consistent background noise baselines (presented in the remaining colours). The baseline level is due to scattering of 980-nm excitation. **b**, Normalized nanocrystal emission integrated from ~800 to 810 nm. The four positive trials shown in red, magenta, dark red and orange produce intensities of ~250 with a low coefficient of variation (CV) of 4.7%, and high signal-to-noise ratio of >8. **c**, Time-dependent dynamics of three independent trials. Red: trial with no nanocrystals observed (only background is observed). Blue: one nanocrystal appears shortly after the start of the trial. Black: single nanocrystal appears in the fibre after 2 min, followed by a second at ~5 min; one of the nanocrystals then exits the observation volume.

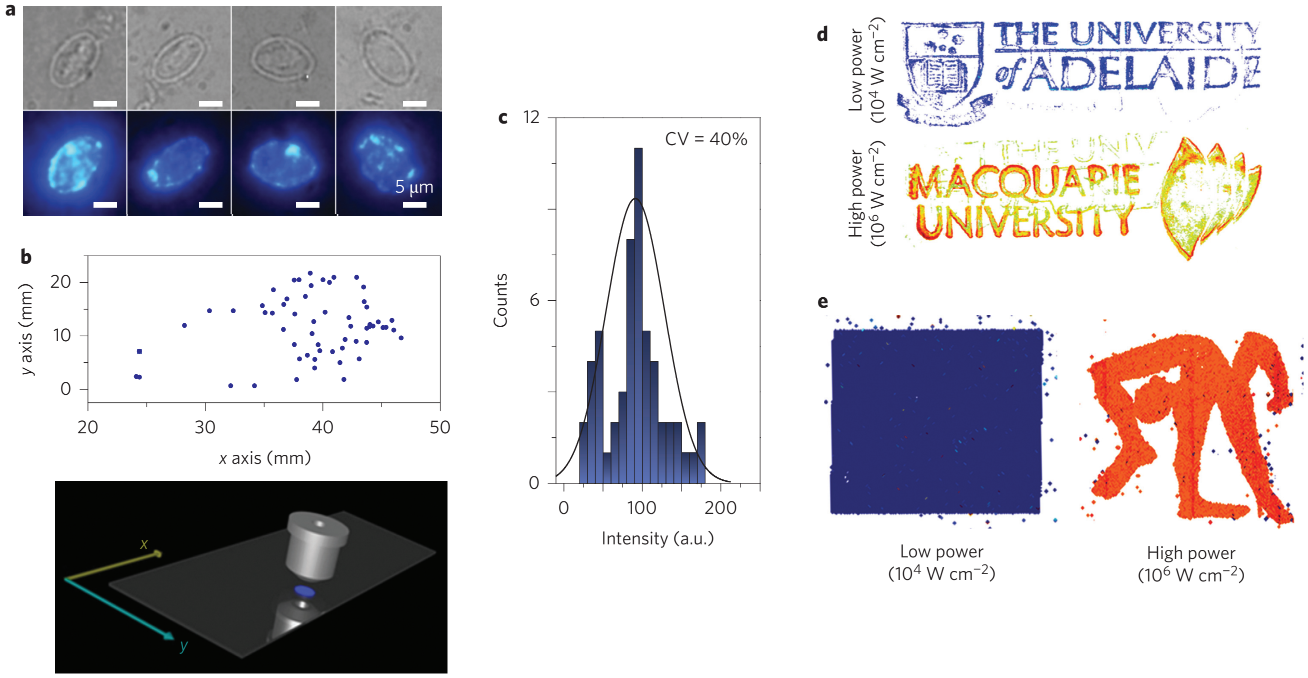

Figure 5 | Proof-of-principle experiments demonstrating a broad spectrum of applications. a, Images of *Giardia lamblia* cells labelled with antibody-conjugated 4 mol% Tm^{3+} upconversion nanocrystals under transmission (top) and luminescence (bottom) modes. The 980-nm wide-field excitation and upconversion detection yield negligible autofluorescence background, so absolute signal intensities of each single microorganism (see histogram in **c**) provide quantification of the level of surface antigens. **b**, Individual cells localized on a glass slide by a scanning cytometry system (top), and its schematic (bottom). Targeted cells are symbolized by blue dots. **c**, Histogram showing the quantification results of the population of nanocrystal-labelled *Giarida lamblia* (CV, coefficient of variation). **d**, Demonstrations of security inks using the power-dependent optimal Tm^{3+} concentration. Low-concentration (0.2 mol% Tm^{3+}) nanocrystals were used to stain the masking pattern (University of Adelaide logo), which is visible under both low-power illumination (top) and high-power illumination (bottom). High-concentration (4 mol% Tm^{3+}) nanocrystals were used to stain the hidden pattern (Macquarie University logo), which is over 10 times brighter than the masking pattern. At this dynamic range the masking pattern is almost unnoticeable. **e**, Nanocrystal solution 'security inks' were used in an inkjet printer with 0.5 mol% Tm^{3+} nanocrystals as a rectangular mask to confound the signal image from 8 mol% Tm^{3+} nanocrystals. At laser scanning confocal setting ($>1 \times 10^6$ W cm^{-2}), the hidden trademark image of the 8 mol% Tm^{3+} nanocrystals becomes visible and dominant.

high irradiance, in agreement with our observations (Supplementary Fig. S9b–f). Moreover, the simulations show increasing relative upconversion efficiency with increasing excitation irradiance (Supplementary Fig. S9g), which is in agreement with Fig. 3a. To the best of our knowledge, this is the first analytical approach to describe the upconversion quenching process at increasing activator concentrations and excitation powers.

We have demonstrated that these bright nanocrystals can significantly extend the detection limit in a fibre-based dip sensor, a novel nanoscale sensing platform for clinical point-of-care, chemical and biological applications[17]. The detection limit for fluorescent quantum dots in such sensors was earlier reported to be ~10 pM due to competing autofluorescence background from the fibre itself. In this work the fibre autofluorescence problem is avoided by using 980 nm excitation and 802 nm emission of Tm^{3+}, wavelengths that are well separated from the glass background fluorescence (Supplementary Fig. S11). To investigate the achievable detection limit, we measured our brightest 8 mol% Tm^{3+} nanocrystals at 3.9 fM dilution in ten identical fibre dip sensors (Supplementary Section S8). The respective 802 nm peaks (Fig. 4a) show a consistent intensity of 250 ± 30 counts in four experiments, whereas six other experiments show a consistent background level of ~30 counts (Fig. 4b). We attribute these strongly quantized values of the peak intensity (~220 net counts) to the observation of single nanocrystals in these four trials. To confirm this hypothesis we calculated the average number of particles expected to be located within the detection volume in a microstructured fibre, and found this to be 0.55, consistent with our observations of a single nanocrystal in 40% of trials. The Poissonian probability of observing two or more nanocrystals in a single trial for our average of 0.55 particles is 11%. To validate our assignment further, we set up an experiment to continuously monitor the 802 nm upconversion intensity during sample intake as the holes of the fibre fill with the nanocrystal suspension by capillary action (Fig. 4c). One of these trials (red) showed the background signal only, indicating that in this trial no nanocrystals entered the detection volume. The second (blue) showed a single nanocrystal appearing in the detection volume halfway through the experiment. The third (black) showed one nanocrystal entering the detection region, followed by a second one after 6 min; one nanocrystal is then observed to exit while the other continues to be observed. The signal of both combined nanocrystals is 470 ± 30 (440 net counts), twice the single nanocrystal net count of 220. These experiments show that high brightness of upconversion emission achieved at sufficient irradiance excitation enables, for the first time, the detection of a single high Tm^{3+}-doped nanocrystal within the fibre platform. Furthermore, these single nanocrystals are bright enough to be visible to the naked eye and could be recorded by a low-cost digital camera in a wide-field microscopy system (Fig. S10 in Supplementary Section S7).

This exceptional nanocrystal brightness provides compelling advantages to a wide range of fields including immunofluorescence imaging (Fig. 5a), rare event cell detection and quantification (Fig. 5b,c), document security (Fig. 5d) and security printing (Fig. 5e). We demonstrated that the new ultrabright upconversion nanocrystals provide high-contrast biolabels. To this end, *Giardia lamblia* cells were labelled by nanocrystals conjugated to suitable monoclonal antibodies (G203). Figure 5a shows the labelled Giardia cells imaged by a scanning system at only 0.1 s exposure time by a standard charge-coupled device (CCD) camera. The absence of autofluorescence background at 980 nm excitation enabled the quantification of the absolute signal intensities of each single microorganism, as well as quantification of the level of surface antigens (Fig. 5c)[33]. Single labelled cells on a glass slide have been detected within 3 min without background interference (Fig. 5b). This shows that these bioprobes are capable of rare event detection. Moreover, excitation-dependent upconversion has also enabled a new approach to 'security inks' (Fig. 5d,e), because the highly doped (>4 mol%) Tm^{3+} nanocrystals remain dark unless high infrared excitation irradiance is used, in contrast to low doped nanocrystals (Fig. 5d). Additionally, the nanocrystal suspensions can be dispersed in traditional inkjet printer inks to print highly secure trademarks/images on papers/plastics (Fig. 5e).

In conclusion, we have demonstrated a novel approach to significantly enhance the upconversion luminescence of nanocrystals, by increasing the activator concentration in combination with elevated irradiance excitation ($\sim 1 \times 10^6$ W cm^{-2}). The microstructured fibre dip sensor used here easily achieves such excitation intensities, making it possible to detect single nanocrystals while probing subcellular fluid volumes. These results show that the nanocrystals can be detected at one end of the fibre as they enter the fibre from the other end, enabling measurements to be made from a significant distance, and leading the way to *in vivo* measurements. Highly Ln^{3+}-doped nanocrystals at sufficient irradiance excitation have strong potential for use as photostable, background-free and extremely bright labelling probes for bioimaging. Furthermore, this work presents a new approach for understanding and predicting the behaviour of lanthanide-based upconversion systems, and provides new directions both for nanoscale sensing and the materials science of Ln^{3+}-doped nanomaterials.

Received 13 May 2013; accepted 26 July 2013;

References

1. Zhang, C., Yuan, Y., Zhang, S., Wang, Y. & Liu, Z. Biosensing platform based on fluorescence resonance energy transfer from upconverting nanocrystals to graphene oxide. *Angew. Chem. Int. Ed.* **50,** 6851–6854 (2011).
2. Wu, S. W. *et al.* Non-blinking and photostable upconverted luminescence from single lanthanide-doped nanocrystals. *Proc. Natl Acad. Sci. USA* **106,** 10917–10921 (2009).
3. Stepuk, A. *et al.* Use of NIR light and upconversion phosphors in light-curable polymers. *Dental Mater.* **28,** 304–311 (2012).
4. Nyk, M., Kumar, R., Ohulchanskyy, T. Y., Bergey, E. J. & Prasad, P. N. High contrast *in vitro* and *in vivo* photoluminescence bioimaging using near infrared to near infrared up-conversion in Tm^{3+} and Yb^{3+} doped fluoride nanophosphors. *Nano Lett.* **8,** 3834–3838 (2008).
5. Wang, M. *et al.* Immunolabeling and NIR-excited fluorescent imaging of HeLa cells by using $NaYF_4$:Yb,Er upconversion nanoparticles. *ACS Nano* **3,** 1580–1586 (2009).
6. Yang, Y. M. *et al. In vitro* and *in vivo* uncaging and bioluminescence imaging by using photocaged upconversion nanoparticles. *Angew. Chem. Int. Ed.* **51,** 3125–3129 (2012).
7. Tian, G. *et al.* Mn^{2+} dopant-controlled synthesis of $NaYF_4$:Yb/Er upconversion nanoparticles for *in vivo* imaging and drug delivery. *Adv. Mater.* **24,** 1226–1231 (2012).
8. Haase, M. & Schäfer, H. Upconverting nanoparticles. *Angew. Chem. Int. Ed.* **50,** 5808–5829 (2011).
9. Auzel, F. Upconversion and anti-Stokes processes with *f* and *d* ions in solids. *Chem. Rev.* **104,** 139–173 (2004).
10. Zou, W. Q., Visser, C., Maduro, J. A., Pshenichnikov, M. S. & Hummelen, J. C. Broadband dye-sensitized upconversion of near-infrared light. *Nature Photon.* **6,** 560–564 (2012).
11. Wang, F. *et al.* Simultaneous phase and size control of upconversion nanocrystals through lanthanide doping. *Nature* **463,** 1061–1065 (2010).
12. Vetrone, F., Naccache, R., Mahalingam, V., Morgan, C. G. & Capobianco, J. A. The active-core/active-shell approach: a strategy to enhance the upconversion luminescence in lanthanide-doped nanoparticles. *Adv. Funct. Mater.* **19,** 2924–2929 (2009).
13. Liu, X. *et al.* Breakthrough in concentration quenching threshold of upconversion luminescence via spatial separation of the emitter doping area for bio-applications. *Chem. Commun.* **47,** 11957–11959 (2011).
14. Boyer, J. C. & van Veggel, F. C. Absolute quantum yield measurements of colloidal $NaYF_4$: Er^{3+}, Yb^{3+} upconverting nanoparticles. *Nanoscale* **2,** 1417–1419 (2010).
15. Wang, F. & Liu, X. Upconversion multicolor fine-tuning: visible to near-infrared emission from lanthanide-doped $NaYF_4$ nanoparticles. *J. Am. Chem. Soc.* **130,** 5642–5643 (2008).
16. Zhang, H., Li, Y., Lin, Y., Huang, Y. & Duan, X. Composition tuning the upconversion emission in $NaYF_4$:Yb/Tm hexaplate nanocrystals. *Nanoscale* **3,** 963–966 (2011).
17. Schartner, E. P., Ebendorff-Heidepriem, H., Warren-Smith, S. C., White, R. T. & Monro, T. M. Driving down the detection limit in microstructured fiber-based chemical dip sensors. *Sensors* **11,** 2961–2971 (2011).
18. Wang, F. *et al.* Tuning upconversion through energy migration in core–shell nanoparticles. *Nature Mater.* **10,** 968–973 (2011).
19. Ye, X. C. *et al.* Morphologically controlled synthesis of colloidal upconversion nanophosphors and their shape-directed self-assembly. *Proc. Natl Acad. Sci. USA* **107,** 22430–22435 (2010).
20. Yan, C., Dadvand, A., Rosei, F. & Perepichka, D. F. Near-IR photoresponse in new up-converting CdSe/$NaYF_4$:Yb,Er nanoheterostructures. *J. Am. Chem. Soc.* **132,** 8868–8869 (2010).

21. Gorris, H. H., Ali, R., Saleh, S. M. & Wolfbeis, O. S. Tuning the dual emission of photon-upconverting nanoparticles for ratiometric multiplexed encoding. *Adv. Mater.* **23,** 1652–1655 (2011).
22. Wang, F., Wang, J. A. & Liu, X. G. Direct evidence of a surface quenching effect on size-dependent luminescence of upconversion nanoparticles. *Angew. Chem. Int. Ed.* **49,** 7456–7460 (2010).
23. Mai, H. X., Zhang, Y. W., Sun, L. D. & Yan, C. H. Highly efficient multicolor up-conversion emissions and their mechanisms of monodisperse $NaYF_4$:Yb,Er core and core/shell-structured nanocrystals. *J. Phys. Chem. C* **111,** 13721–13729 (2007).
24. Priyam, A., Idris, N. M. & Zhang, Y. Gold nanoshell coated $NaYF_4$ nanoparticles for simultaneously enhanced upconversion fluorescence and darkfield imaging. *J. Mater. Chem.* **22,** 960–965 (2012).
25. Zhang, F. *et al.* Fabrication of Ag@SiO_2@Y_2O_3:Er nanostructures for bioimaging: tuning of the upconversion fluorescence with silver nanoparticles. *J. Am. Chem. Soc.* **132,** 2850–2851 (2010).
26. Yin, A., Zhang, Y., Sun, L. & Yan, C. Colloidal synthesis and blue based multicolor upconversion emissions of size and composition controlled monodisperse hexagonal $NaYF_4$:Yb,Tm nanocrystals. *Nanoscale* **2,** 953–959 (2010).
27. Mahalingam, V., Vetrone, F., Naccache, R., Speghini, A. & Capobianco, J. A. Colloidal Tm^{3+}/Yb^{3+}-doped $LiYF_4$ nanocrystals: multiple luminescence spanning the UV to NIR regions via low-energy excitation. *Adv. Mater.* **21,** 4025–4028 (2009).
28. Kramer, K. W. *et al.* Hexagonal sodium yttrium fluoride based green and blue emitting upconversion phosphors. *Chem. Mater.* **16,** 1244–1251 (2004).
29. Liang, L. F., Wu, H., Hu, H. L., Wu, M. M. & Su, Q. Enhanced blue and green upconversion in hydrothermally synthesized hexagonal $NaY_{1-x}Yb_xF_4$:Ln^{3+}. *J. Alloys Comp.* **368,** 94–100 (2004).
30. Chen, X. & Song, Z. Study on six-photon and five-photon ultraviolet upconversion luminescence. *J. Opt. Soc. Am. B* **24,** 965–971 (2007).
31. Chen, G. Y., Somesfalean, G., Zhang, Z. G., Sun, Q. & Wang, E. P. Ultraviolet upconversion fluorescence in rare-earth-ion-doped Y_2O_3 induced by infrared diode laser excitation. *Opt. Lett.* **32,** 87–89 (2007).
32. Qin, G. S. *et al.* Intense ultraviolet upconversion luminescence from Yb^{3+} and Tm^{3+} codoped amorphous fluoride particles synthesized by pulsed laser ablation. *Opt. Commun.* **242,** 215–219 (2004).
33. Lu, Y., Xi, P., Piper, J. A., Huo, Y. & Jin, D. Time-gated orthogonal scanning automated microscopy (OSAM) for high-speed cell detection and analysis. *Sci. Rep.* **2,** 837 (2012).

Acknowledgements

The authors thank D. Birch, D. Inglis, N. Vella, A. Nadort, R. Field, M. Nguyen, D. Liu, C. Yan and J. Shen (Olympus Australia) for sample characterization, H. Ebendorff-Heidepriem for providing the suspended-core fibres, which were fabricated at the OptoFab node of the Australian National Fabrication Facility (ANFF), and A. Nechaev (Lomonosov Moscow State University of Fine Chemical Technologies, Russia) for bulk crystal preparation. J.Z. acknowledges a Macquarie University Research Excellence Scholarship, and D.J. and J.P. acknowledge support from the Australian Research Council (DP1095465, LP130100517). P.X. acknowledges support from the '973 program' of China (2011CB707502, 2011CB809101) and T.M. acknowledges the support of an ARC Federation Fellowship.

Author contributions

D.J. and T.M. conceived the project, designed the experiments and supervised the research. J.Z., E.S., Y.Lu and D.J. were primarily responsible for data collection and analysis. D.J., E.G., J.Z. and T.M. prepared figures and wrote the main manuscript text. J.Z., E.G., A.Z. and D.J. were primarily responsible for supporting information and numerical simulations. All authors contributed to data analysis, discussions and manuscript preparation.

Additional information

Supplementary information is available in the online version of the paper. Reprints and permissions information is available online at www.nature.com/reprints. Correspondence and requests for materials should be addressed to D.J.

Competing financial interests

The authors declare no competing financial interests.